Available online at www.sciencedirect.com

ScienceDirect

Current Opinion in Behavioral Sciences

High-resolution fMRI at 7 Tesla: challenges, promises and recent developments for individual-focused fMRI studies

Olivia Viessmann[1,2] and Jonathan R Polimeni[1,2,3]

Limited detection power has been a bottleneck for subject-specific functional MRI (fMRI) studies; however, the higher signal-to-noise ratio afforded by ultra-high magnetic fields (≥7 Tesla) provides levels of sensitivity and resolution needed to study individual subjects. What may be surprising is that higher imaging resolution may provide both higher specificity and sensitivity due to reductions in partial volume effects and reduced physiological noise. However, challenges remain to ensure high data quality and to reduce variability in ultra-high field fMRI. We discuss session-specific *biases* including those caused by factors related to instrumentation, anatomy, and physiology—which can translate into *variability* across sessions—and how to minimize these to help ultra-high field fMRI reach its full potential for individual-focused studies.

Addresses
[1] Athinoula A. Martinos Center for Biomedical Imaging, Massachusetts General Hospital, Charlestown, MA, USA
[2] Department of Radiology, Harvard Medical School, Boston, MA, USA
[3] Division of Health Sciences and Technology, Massachusetts Institute of Technology, Cambridge, MA, USA

Corresponding author:
Viessmann, Olivia (oviessmann@mgh.harvard.edu)

Current Opinion in Behavioral Sciences 2021, **40**:96–104

This review comes from a themed issue on **Deep imaging - personalized neuroscience**

Edited by **Caterina Gratton** and **Rodrigo Martin Braga**

https://doi.org/10.1016/j.cobeha.2021.01.011

2352-1546/© 2021 Elsevier Ltd. All rights reserved.

Introduction

In magnetic resonance imaging (MRI), image signal-to-noise ratio (SNR) increases with increasing magnetic field strength [1]. This higher sensitivity allows for acquisition strategies that enable higher image quality and resolution [2]. Additionally, higher field strength enhances magnetic susceptibility-based contrast, such as the blood-oxygenation-level dependent (BOLD) contrast—the most common contrast used for functional MRI (fMRI). The boost in functional contrast-to-noise ratio (fCNR) in BOLD has made fMRI a key application of ultra-high field (UHF) MRI at field strengths of 7 Tesla (7 T) and above [3]. This sensitivity boost enables studies of fine-scale functional architecture, such as cortical columns, layers, and subcortical nuclei [4–6] and also increases statistical power needed for single-subject analysis. As discussed elsewhere in this *Special Issue*, a central motivation behind group studies in neuroimaging is to increase sensitivity to detect subtle functional features by averaging across subjects. However, meaningful individual differences, in structure or functional organization, can smear out these features when averaging across subjects. Thus the increased statistical power of BOLD-fMRI at UHF may also help enable the detection of subject-specific activation patterns in individuals.

UHF-fMRI, however, has its challenges. Several well-known fMRI artifacts increase in severity with field strength, and several subtle sources of bias are amplified—which, if unaddressed, can reduce sensitivity and counteract the gains of moving to higher fields. So, do the benefits of UHF-fMRI outweigh the costs? To address this question, here we review new technologies that improve UHF-fMRI quality and survey sources of bias. Notably, biases and artifacts can vary both within and across experimental sessions and thereby contribute variance or 'noise'. We discuss how these sources of variance can be identified, characterized, and minimized. If these challenges are addressed, UHF-fMRI can be a powerful tool for individual-focused studies.

Benefits of 7 T fMRI for individual-focused fMRI studies

The motivation behind individual-focused fMRI at UHF can be appreciated by reviewing the studies performed to date. In a pair of influential studies, first conducted at 3 T then repeated at 7 T, whole-brain activation to a simple visual stimulus was measured after averaging 100 runs across 10 experimental sessions [7••,8•]. Figure 1a summarizes how the measured activation pattern increasingly extended across the entire brain as more runs were included, well beyond the expected visual cortical and subcortical regions. The large number of samples allowed them to use trial-locked averaging, and this 'unconstrained' analysis uncovered meaningful activations that are missed by conventional model-based analysis. The lesson was that meaningful activations that do not match our models may go undetected, leading to what they referred to as a pervasiveness of false negatives in

Figure 1

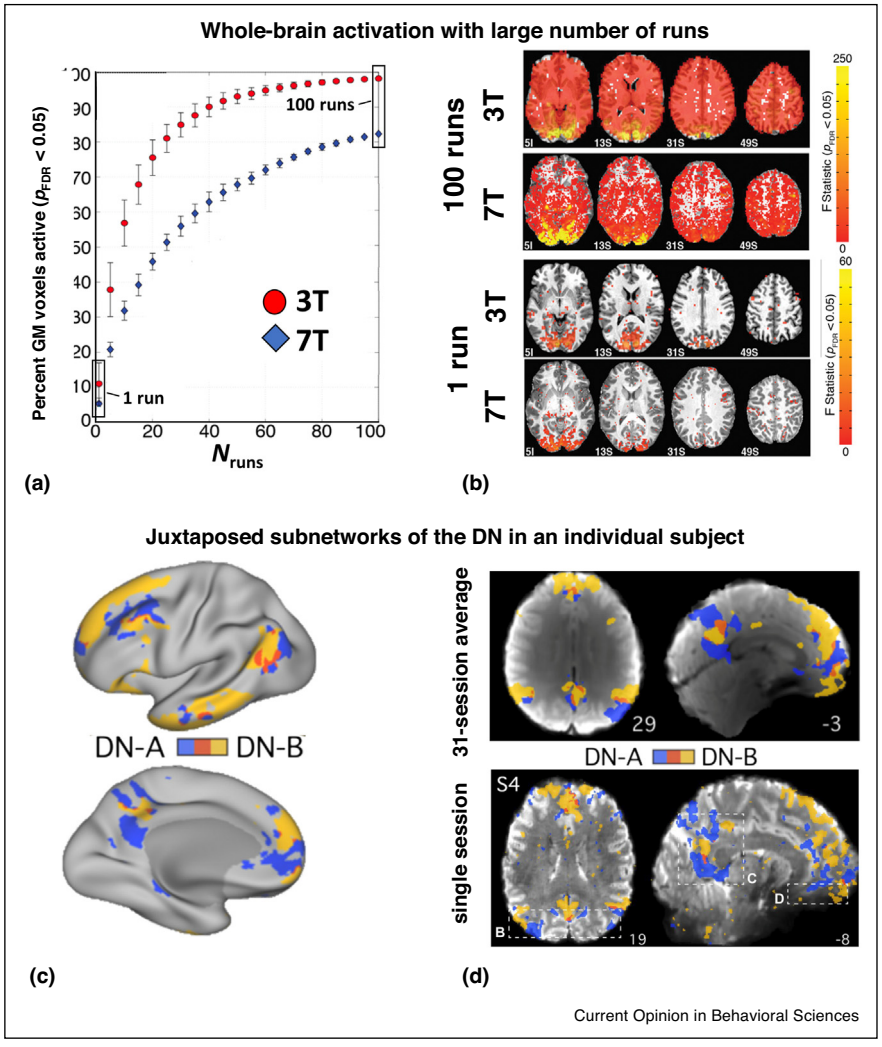

Examples of novel insights from a highly powered single-subject 7 T fMRI data.
(a),**(b)** Gonzalez-Castillo *et al.* show how time-locked model-free analysis of BOLD-fMRI data can reveal whole-brain activation. The average task-related activation pattern extends beyond the visual areas with an increasing number of runs. The 7 T activation pattern is more confined to the gray matter compared to 3 T. (Adapted from Ref. [8•].) **(c)** Braga *et al.* reveal how the Default Network fractionates into two spatially separated subnetworks within the individual using 31 sessions of resting-state BOLD-fMRI at 3 T. (Adapted from Ref. [12].) **(d)** They repeated their study at 7 T where they can reveal the network separation within the individual from a single session of 24 min worth of data. (Adapted from Ref. [12].).

standard studies. At 7 T this analysis revealed activations that were more focal and contained within the cortical gray matter compared to 3 T (see Figure 1b).

Similarly, a well-known pair of highly powered studies of individual subjects demonstrated that consistent patterns of functional connectivity were only achievable by pooling over 100 min of resting-state fMRI data acquired over many experimental sessions at 3 T [9•,10]. These studies revealed idiosyncratic functional connectivity patterns in individuals that were not seen at the group level. They concluded that *between-session variability* is dwarfed by *between-subject variability*, and that this inter-individual variability is a dominant confound in group-level differences. We return to the topic of between-session variability further below.

Another pair of highly powered studies of individual subjects revealed subject-specific patterns of subnetworks that challenge widely held theories of brain network organization. Again first conducted at 3 T over 24 experimental sessions [11••] and then replicated at 7 T [12], the Default Network (DN) was found to fractionate into two independent spatially interdigitated subnetworks, shown in Figure 1c. The broad anatomical location of the networks was conserved

across subjects, but the subnetwork spatial pattern details showed features idiosyncratic to the subject that were consistent across sessions. These subnetworks disappeared when the data were pooled across subjects [11••]. Remarkably, these same subnetworks were observable in the individual from a single experimental session at 7 T [12], showcasing the ability of 7 T to provide sufficient sensitivity for single-subject fMRI. Figure 1d shows the subnetworks of an individual derived from 7 T data, where the fine-scale detail can be appreciated.

Individual-focused fMRI is an emerging direction for whole-brain fMRI studies, but it is standard for studies of meso-scale functional architecture such as cortical columns [13–16], as the precise spatial layouts of these patterns are expected to be unique to the individual and thus require single-subject analysis. Although these high-resolution fMRI studies are performed at UHF, because mapping columns often requires detection of subtle differences in functional activation, extensive averaging is still required. One recent study into the interdigitated columnar system in human visual cortex showcased the ability to resolve these fine-scale details only when sufficient BOLD-fMRI data from multiple sessions were carefully acquired and analyzed [16]. This is somewhat analogous to the abovementioned study revealing interdigitated subnetworks by carefully pooling data across sessions [11••].

Moving from 3 T to 7 T increases sensitivity only if small fMRI voxels are used—and in fact one may experience a sensitivity loss at 7 T if large fMRI voxels are used! This is because physiological noise, which is a structured noise fluctuation in the fMRI signal, also increases with field strength [17], diminishing sensitivity gains. However, small fMRI voxels have reduced physiological noise and are thermal-noise dominated; therefore, high-resolution fMRI acquisitions enjoy the expected sensitivity boost at higher field [18•,19]. The critical voxel-size cutoff for thermal noise dominance depends on several factors [19]; however, a rough estimate for an upper threshold for BOLD-fMRI is 1.5 mm isotropic, and studies using voxels larger than this threshold may not benefit when moving from 3 T to 7 T.

One may then ask whether conventional studies that do not require high resolution per se would benefit from moving to higher field. While general recommendations are difficult to make, reducing voxel size can also benefit these conventional studies. This is because smaller voxel sizes reduce partial volume effects, allowing the voxels to sample gray matter more exclusively. Perhaps surprisingly, small-voxel fMRI with advanced anatomically informed smoothing can provide higher overall sensitivity and fCNR than conventional large-sized voxels [20•]. Therefore, acquiring fMRI data with voxels small enough to adequately sample the cortex is advantageous even for conventional studies investigating large-scale brain organization. Below we discuss further strategies to reduce other noise sources including across-run and between-session variability, which can also increase with field strength.

High-performance EPI at 7 T

The most widely used acquisition method for fMRI is echo-planar imaging (EPI). The main limitation of EPI is geometric distortion and blurring along the phase-encoding direction. This distortion predominantly arises from magnetic field inhomogeneities caused by tissue susceptibility gradients. The severity increases with field strength and can produce centimeters of artifactual tissue displacement in the brain at 7 T. The most effective tool to minimize distortions is accelerated parallel imaging, which increases the encoding bandwidth in the phase-encoding direction. Parallel imaging performance increases with field strength [21] and modern Radio Frequency (RF) receive coil arrays [22,23] and acceleration factors up to $R = 4$ are feasible. The distortion reduction with acceleration and improvement in data quality can be seen in Figure 2a.

Acceleration also enables higher imaging resolution in EPI, thus parallel imaging is used ubiquitously in UHF-fMRI. Several recent pulse sequence and image reconstruction advances provide enhanced image quality and practical usability of high-resolution EPI, including improvements in motion robustness, reliability of highly accelerated EPI [24–26] and reduction of subtle artifacts seen in UHF-fMRI [27,28]. Additionally these high-performance EPI methods can reduce within-run and across-run variability because these artifacts can vary over time [27,29] (see Figure 2b). Implementing these technologies requires changes to the acquisition software, which requires specific expertise and resources; however, several of these technologies listed above are now available on some UHF platforms, provided either by the vendor or freely distributed by research centers.

Another more overlooked source of variability is dynamic distortion in EPI. This is caused by an interaction between head motion and magnetic field inhomogeneity [30]. Motion causes distortion changes because the field offsets are a function of head orientation within the B_0 field [31]. Available post-processing correction techniques either estimate and correct the temporally varying magnetic field patterns [32,33] or jointly estimate head motion and distortion [34]. Correcting dynamic distortions during the acquisition may be possible by combining dynamic field sensing [35,36], field control [37,38] and prospective motion correction [39,40]; several MR instrumentation companies offer these hardware-based solutions; however, there are still challenges in integrating these into standard workflows for routine imaging. Motion

Figure 2

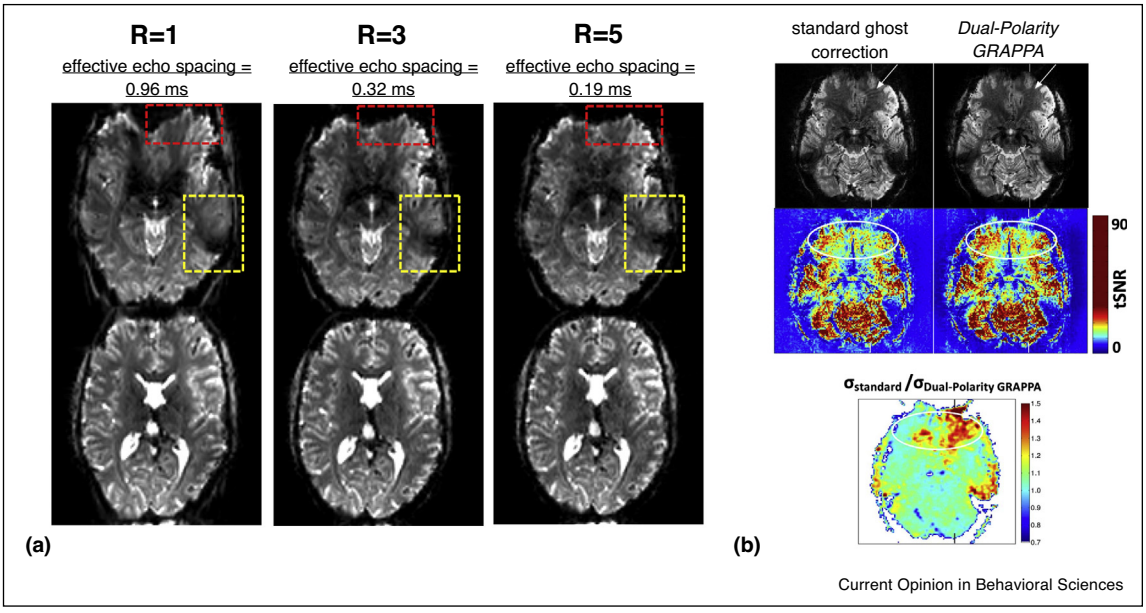

Geometric distortion in EPI for different parallel acceleration factors and reconstruction strategies.
(a) The unaccelerated ($R = 1$) image shows severe distortion in particular in the frontal area (red box) and the ear canals (yellow box). With increased acceleration the effective echo spacing decreases (which increases the bandwidth in the phase-encoding direction) leading to reduced vulnerability to distortion. **(b)** Advanced reconstruction methods for parallel imaging (here, Dual-Polarity GRAPPA or DPG) reduce ghosting artifacts that vary over time, thereby improving the temporal stability of the fMRI data. Reduced interference pattern artifacts are seen near to regions of B_0 inhomogeneity (white arrows) in DPG reconstruction, and the artifact changes slightly over time. Temporal SNR (tSNR) maps show higher sensitivity in DPG reconstruction in this same region after artifact removal. Below the ratio of the time-series instability of the standard and DPG reconstructions is shown, demonstrating improved temporal stability in the DPG reconstruction. (Adapted from Ref. [27].).

suppression using custom head holders can also help minimize this challenging artifact [41,42].

The MRI scanner instrumentation places limits on the achievable imaging resolution and it is not always possible to acquire the desired spatial resolution, demanding new advances in MRI hardware (as recently reviewed in Ref. [43]). Exciting innovations in UHF-fMRI instrumentation are ongoing [23,38,44], and are expected to have a major impact on imaging capabilities once they become widely available.

Bias from MRI instrumentation

Several sources of instrumentation bias become pronounced at higher field and cause spatially varying fMRI sensitivity that induces between-session variability. The most well-known and perhaps strongest bias stems from the RF receive coil array. The receive sensitivity, or the B_1^- field, is highest closest to the detector and falls off steeply with distance [45] and thus detectability is maximal at the brain periphery and lowest at the center. Figure 3a shows the average B_1^- field in the standard 32-channel RF coil at 7 T, with an eightfold variation seen across the brain. This causes a position-dependent detection bias for high-resolution fMRI where the small voxels are thermal-noise dominated [46]. This also interacts with motion as the head moves through the spatially varying coil sensitivity [47,48]. While correction techniques have been proposed [48], motion suppression may be the most effective solution. Inconsistent subject repositioning between sessions will cause sensitivity-induced variance; Figure 3b demonstrates how the B_1^- field varies up to 13% for a given subject between sessions. However, this within-subject variability is lower than across-subject variability as shown in Figure 3c, indicating that the across-subject differences in brain anatomy/geometry and differences in head placement contribute more to B_1^- variability.

A related but distinct bias source stems from the RF transmit coil. With increasing field strength the RF transmit or B_1^+ field becomes more spatially nonuniform due to dielectric effects. In practice this leads to a spatially varying flip angle, which can also cause a position-dependent fMRI detection bias in thermal-noise-dominated acquisitions [49]. It is impossible to achieve the desired flip angle over the entire brain, but one can either optimize the B_1^+ field for a given region of interest (at the expense of others) or calibrate such that acceptable flip angles are achieved across the brain. This calibration procedure is vendor

Figure 3

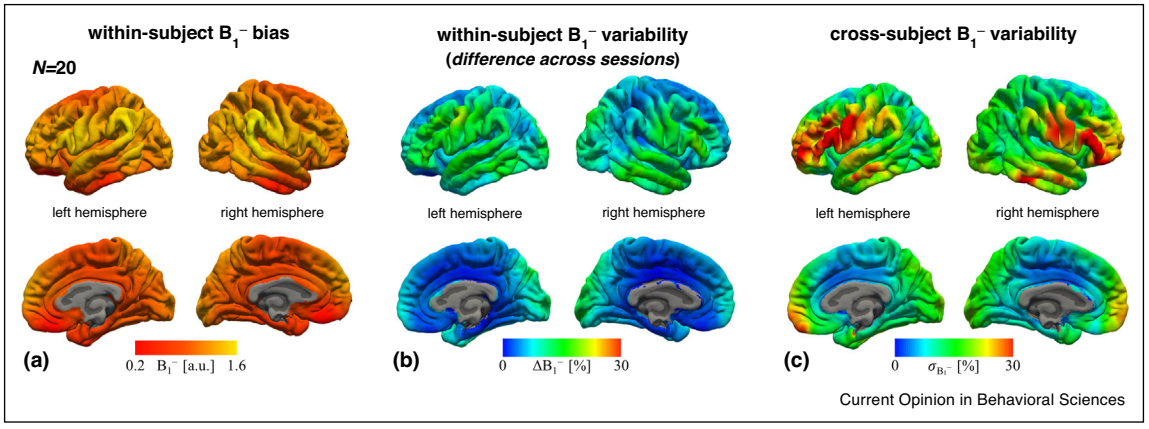

Example receive coil or B_1^- fields on within- and across-subject variability.
B_1^- field estimated for a standard 7 T 32-channel coil array (derived from 20 subjects). **(a)** The B_1^- profile averaged across subjects shows a nearly eightfold spatial variation in receive sensitivity, with folds closest to the periphery exhibiting consistently higher sensitivity. **(b)** The average difference in B_1^- profile between two sessions. The temporal lobes and folds in the periphery exhibit the highest difference in receive field sensitivity when the subject is repositioned in the scanner. The pattern of the B_1^- between-session difference is distinct from the average B_1^- profile, which likely reflects an interaction between the steep B_1^- profile of this coil array and the variability in head positioning, which itself will depend on the operator and on the coil array housing. **(c)** The B_1^- profile variability across subjects. The pattern of the variability of the B_1^- profile across subjects is similar to the between-session difference for the single subject, but 2–3 times more severe, likely because of the additional variability of brain geometry across subjects. This is particularly observable in the front of the brain which likely reflects the variation of the distance between forehead and the coil housing across subjects.

specific, and may require intervention by the scanner operator to ensure optimal B_1^+ settings.

A final form of bias stems from gradient nonlinearity. MR image encoding assumes linear magnetic field gradients imposed over space by the gradient coils. Perfect linearity cannot be achieved in practice and there is spatially varying nonlinearity in the gradient field. This causes geometric image distortion and spatially varying voxel sizes. The gradient is linear close to the scanner isocenter but typically becomes nonlinear about 10 cm offcenter. Fortunately this gradient nonlinearity is determined by the gradient coil and is constant; therefore, it is straightforward to account for in postprocessing [50•]. Nevertheless, when comparing data across sessions, when the head may be in different positions relateive to the isocenter, gradient nonlinearity correction will be required to remove differential distortion. Changes in head position during an experimental session can also cause differential distortion in brain areas near to the regions of nonlinear gradients.

All of these three sources of bias—RF receive field (B_1^-), RF transmit field (B_1^+) and gradient non-linearities—are impacted by head positioning, and, therefore, each will vary across experimental sessions, introducing between-session variability. While B_1^- and B_1^+ fields can be estimated with relatively short acquisitions, and gradient nonlinearity fields are often provided by the manufacturer, these biases are not commonly addressed. One simple solution, analogous to motion suppression, is consistent head positioning across sessions, including positioning within the RF coil housing as well as landmarking of the subject and positioning of the patient table relative to the magnet isocenter. Custom-molded foam padding can help ensure consistent head placement, and has recently been used to minimize bias differences across sessions at 3T[4] . Consistent operational procedures for scanner calibration and subject handling can also reduce variability; however, more efforts are needed to provide analysis tools for characterizing and/or removing this variability across sessions.

Anatomical and physiological sources of bias

In addition to bias imposed by instrumentation, there are several subject-specific anatomical/physiological factors that are increasingly understood to impose spatially varying bias on the fMRI signal. Partial volume effects vary across the brain as the tissue geometry changes relative to the voxel grid. For this reason, cortical thickness may impact BOLD contrast and noise [51]. Figure 4 shows the variation in the percentage of the fMRI voxel containing gray matter; the proportion and degree of gray matter voxels showing partial volume effects decreases with

[4] Wang F, Dong Z, Tian Q, Liao C, Fan Q, Hoge WS, Ngamsombat C, Keil B, Polimeni JR, Wald LL, Huang SY, Setompop K: *Proc Intl Soc Mag Reson Med* 2020, 28:0963.

Figure 4

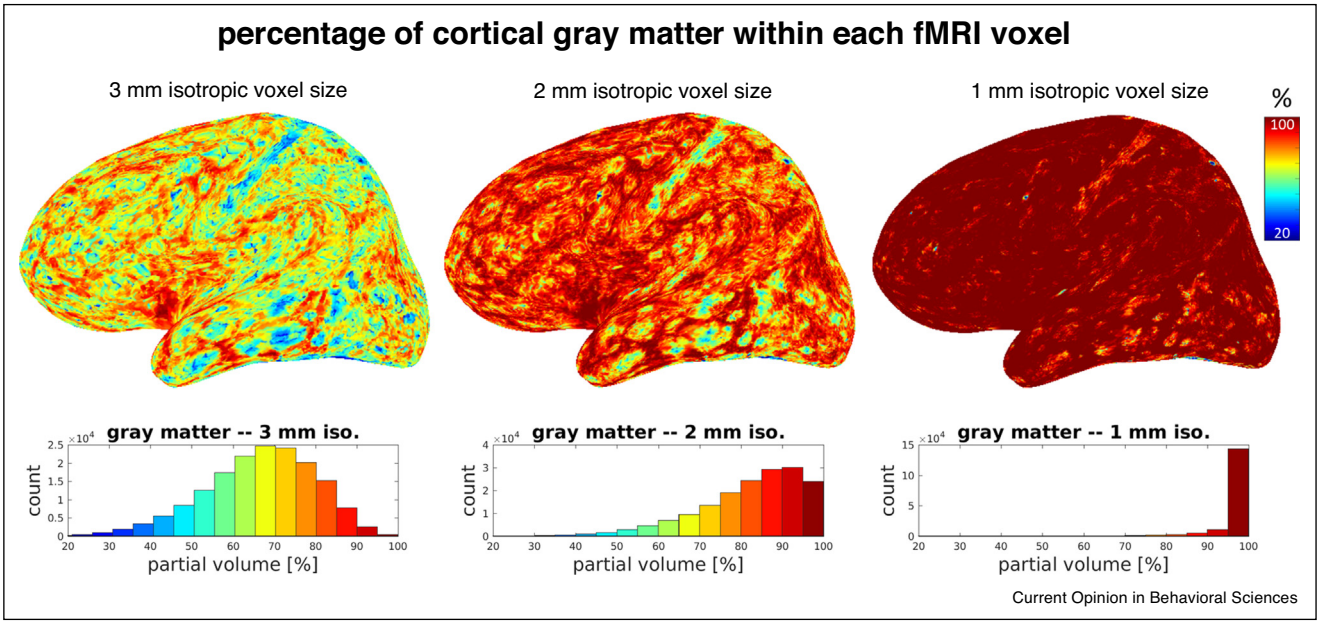

Spatially varying partial volume effects across the brain.
The percentage of gray matter contained within voxels intersecting the surface at mid-cortical depth is plotted across several isotropic voxel sizes, visualized on the inflated surface, with histograms displaying the distribution over the hemisphere. (Partial volume was computed using *FreeSurfer* for multiple fMRI voxel grids at different positions relative to the cortex, then averaged.) For the 3-mm case there are regions where fMRI voxels contain as little as 20% gray matter, while for the 1-mm case the fMRI voxels within nearly every region contain almost 100% gray matter. Thinner cortical regions (such as primary somatosensory cortex) exhibit lower percentages of gray matter. While the spatial heterogeneity of these effects is pronounced for larger voxels, partial volume can be readily estimated in order to take this effect into account during data analysis and interpretation.

smaller voxels, reducing signal dilution from white matter and noise contamination from cerebrospinal fluid.

Other spatially varying biases include the cortical orientation effect, where the coupling between the vascular anatomy and cortical anatomy impart an influence on the BOLD contrast and noise that varies with cortical orientation [52•,53]. This effect also increases with field strength [52•]. Like the instrumentation biases mentioned above, the orientation effect changes with head positioning, posing an additional potential source of between-session variability even in individual-focused studies. Furthermore, vascular anatomy is known to vary substantially across the brain and across individuals [54].

Accounting for spatially varying detection power

The biases discussed above produce spatially varying statistical power that must be accounted for in both single-subject and group-level analysis. Consider a normal distribution of voxels having no effect $N(0,1)$ (null hypothesis) and of voxels having a true effect $N(\sqrt{n}\mu/\sigma, 1)$) where n is the number of samples, μ is the effect size and σ the noise standard deviation. Spatially varying biases impart spatially varying σ and a subsequent variation of statistical power across the brain. Bias-induced variations in σ are substantial, in particular at 7 T. We recently demonstrated that cortical orientation effects in 7 T fMRI data impart a 70% variation in fluctuation amplitudes across the brain [52•], such that a cortical location with parallel surface orientation would thus require $n_{\text{parallel}}/n_{\text{perpendicular}} = 1.7^2 \approx 3$ times the samples to reach equivalent statistical significance compared to a location with perpendicular surface orientation. Biases also impart spatial variability in detectability between sessions and across subjects. Arguably, the between-session variability for an individual is lower than the variability between two subjects because brain geometry contributes to across-subject variability. This can be appreciated in Figure 3b–c, where between-session difference in the B_1^- field within-subjects is shown to be less than the across-subject variability. Thus, for a given effect size, on the basis of B_1^- variability alone a group-level study consisting of single experimental sessions compared to an individual-level study comprising multiple experimental sessions would require roughly $n_{\text{across-subject}}/n_{\text{within-subject}} = (30\%/13\%)^2 \approx 5$ times total more samples to achieve the same statistical power across the entire brain.

This spatially varying detection power may not be a problem for studies that are highly powered, but proper power analysis during experimental design should factor in these effects. Ideally practitioners would have estimates of these biases to help with data interpretation, and to guard against incorrect inference when, for example, an expected effect is seen in a region of the brain with high detection power while an expected effect is not seen in a region with low detection power.

While best-practice scanner operation strategies can reduce variance from both anatomy/physiology and instrumentation, complete elimination is unlikely; therefore, more effort will be required to both account for this variability and to interpret individual-focused fMRI data. For example, analyses could incorporate bias maps to weight the fMRI data or derive confidence limits. Indeed, recent work demonstrated that fMRI reliability is enhanced when across-run variability is accounted for in the general linear model [55], and strategies with explicit measures of biases are expected to improve reliability.

Conclusions and outlook

UHF-fMRI offers increased sensitivity to aid individual-focused studies; however, several sources of variability are enhanced at UHF which give rise to variations in statistical power across the brain as well as variations across sessions and across subjects. Operational strategies exist for minimizing variations of sensitivity over time (i.e. across sessions); however, variations in sensitivity over space (i.e. across the brain) will persist. If these sources of variability are addressed, single-subject UHF-fMRI can achieve higher measurement consistency than group-level studies. This will likely enhance statistical power per sample for single-subject studies: a recent study found that about 30 fMRI runs from two individual subjects at 7 T, analyzed with best-practice methods, produced comparable results to a 181-subject average [56••], meaning in this case 15 times less data were required for the individual compared to the group. UHF-fMRI thus appears ready to provide more information about meaningful individual differences in functional organization [57].

Relevant UHF-fMRI topics that were not discussed here are the potential for higher spatial and temporal resolution [58–60]; increased microvascular specificity of BOLD-fMRI [61]; and the possibility of non-BOLD-fMRI techniques that promise higher neuronal specificity [62]. Also, preprocessing choices influence the final results [63••] and resolution can be inadvertently lost during preprocessing [50•,64]; these losses must be avoided to retain the detailed functional patterns seen in the individual.

Overall, UHF-fMRI is a mature tool whose enhanced sensitivity can contribute greatly to individual-focused neuroscience. It is our hope that the strategies outlined here for addressing the specific challenges of UHF-fMRI encourage future studies that exploit this powerful technology.

Conflict of interest statement

Nothing declared.

CRediT authorship contribution statement

Olivia Viessmann: Conceptualization, Methodology, Formal analysis, Writing - original draft, Writing - review & editing. **Jonathan R Polimeni:** Conceptualization, Methodology, Formal analysis, Writing - original draft, Writing - review & editing.

Acknowledgements

We thank Dr Javier Gonzalez-Castillo and Dr Rodrigo Braga for the permission to reuse published figure material. This work was supported in part by the N.I.H. NIBIB (grants P41-EB030006 and R01-EB019437), NINDS (grant R21-NS106706), NIMH (grant R01-MH124004), by the BRAIN Initiative (NIH NIMH grants R01-MH111419 and R01-MH111438, and NIH NIBIB grant U01-EB025162), and by the MGH/HST Athinoula A. Martinos Center for Biomedical Imaging.

Data were provided by the Human Connectome Project, WU-Minn Consortium (Principal Investigators: David Van Essen and Kamil Ugurbil; U54-MH091657) funded by the 16 NIH Institutes and Centers that support the NIH Blueprint for Neuroscience Research; and by the McDonnell Center for Systems Neuroscience at Washington University.

References and recommended reading

Papers of particular interest, published within the period of review, have been highlighted as:

- • of special interest
- •• of outstanding interest

1. Pohmann R, Speck O, Scheffler K: **Signal-to-noise ratio and MR tissue parameters in human brain imaging at 3, 7, and 9.4 tesla using current receive coil arrays**. *Magn Reson Med* 2016, **75**:801-809.

2. Setsompop K, Feinberg DA, Polimeni JR: **Rapid brain MRI acquisition techniques at ultra-high fields**. *NMR Biomed* 2016, **29**:1198-1221.

3. Polimeni JR, Uludağ K: **Neuroimaging with ultra-high field MRI: present and future**. *Neuroimage* 2018, **168**:1-6.

4. Norris DG, Polimeni JR: **Laminar (f)MRI: a short history and future prospects**. *Neuroimage* 2019, **197**:643-649.

5. De Martino F, Yacoub E, Kemper V, Moerel M, Uludağ K, De Weerd P, Uğurbil K, Goebel R, Formisano E: **The impact of ultra-high field MRI on cognitive and computational neuroimaging**. *Neuroimage* 2018, **168**:366-382.

6. Dumoulin SO, Fracasso A, van der Zwaag W, Siero JCW, Petridou N: **Ultra-high field MRI: advancing systems neuroscience towards mesoscopic human brain function**. *Neuroimage* 2018, **168**:345-357.

7. •• Gonzalez-Castillo J, Saad ZS, Handwerker DA, Inati SJ, Brenowitz N, Bandettini PA: **Whole-brain, time-locked activation with simple tasks revealed using massive averaging and model-free analysis**. *Proc Natl Acad Sci U S A* 2012, **109**:5487-5492.

By measuring whole-brain fMRI activation in response to a simple visual stimulus after averaging 100 runs across 10 experimental sessions, this study demonstrated that with sufficient sensitivity activation can be detected over nearly the entire brain, not merely within the visual cortical and subcortical regions as might be expected. Although model-based analyses are effective at detecting subtle activations that match the model, meaningful activations that do not match our models may go

undetected, leading to what they referred to as a 'pervasiveness of false negatives' in standard studies.

8. • Gonzalez-Castillo J, Hoy CW, Handwerker DA, Roopchansingh V, Inati SJ, Saad ZS, Cox RW, Bandettini PA: **Task dependence, tissue specificity, and spatial distribution of widespread activations in large single-subject functional MRI datasets at 7T**. *Cereb Cortex* 2015, **25**:4667-4677.

The same group later performed a similar study at 7T, acquiring 100 BOLD-fMRI runs in each subject over 11 experimental sessions. At 7T the findings at 3T were replicated, and the detected activations revealed through this analysis were more focal and contained within the cortical gray matter.

9. • Laumann TO, Gordon EM, Adeyemo B, Snyder AZ, Joo SJ, Chen MY, Gilmore AW, McDermott KB, Nelson SM, Dosenbach NUF *et al.*: **Functional system and areal organization of a highly sampled individual human brain**. *Neuron* 2015, **87**:657-670.

This study demonstrated that consistent functional connectivity estimates were achieved only after combining 100 minutes of BOLD-fMRI data acquired over a one-year period, suggesting the possibility that a single dedicated experimental session may suffice to detect unique, subject-specific networks. These data also demonstrated that the highly sampled individual subject exhibited patterns of functional connectivity that differed from the group maps. The authors concluded that inter-individual variability adds noise, and here we can see that just 100 min of data in one subject were sufficient.

10. Gordon EM, Laumann TO, Gilmore AW, Newbold DJ, Greene DJ, Berg JJ, Ortega M, Hoyt-Drazen C, Gratton C, Sun H *et al.*: **Precision functional mapping of individual human brains**. *Neuron* 2017, **95**:791-807.e7.

11. •• Braga RM, Buckner RL: **Parallel interdigitated distributed networks within the individual estimated by intrinsic functional connectivity**. *Neuron* 2017, **95**:457-471.e5.

This study demonstrated, using resting-state BOLD fMRI data acquired at 3T over 24 experimental sessions, that the Default Network was found to be comprised of two independent and spatially interdigitated subnetworks whose spatial patterns were consistent within an individual across sessions but with spatial pattern details that were idiosyncratic to the subject. Similar fractionation was observed in the Fronto-Parietal Control Network and the Dorsal Attention Network within association cortex.

12. Braga RM, Van Dijk KRA, Polimeni JR, Eldaief MC, Buckner RL: **Parallel distributed networks resolved at high resolution reveal close juxtaposition of distinct regions**. *J Neurophysiol* 2019, **121**:1513-1534.

13. Cheng K, Waggoner RA, Tanaka K: **Human ocular dominance columns as revealed by high-field functional magnetic resonance imaging**. *Neuron* 2001, **32**:359-374.

14. Yacoub E, Shmuel A, Logothetis NK, Uğurbil K: **Robust detection of ocular dominance columns in humans using Hahn Spin Echo BOLD functional MRI at 7 Tesla**. *Neuroimage* 2007, **37**:1161-1177.

15. Yacoub E, Harel N, Uğurbil K: **High-field fMRI unveils orientation columns in humans**. *Proc Natl Acad Sci U S A* 2008, **105**:10607-10612.

16. Nasr S, Polimeni JR, Tootell RBH: **Interdigitated color- and disparity-selective columns within human visual cortical areas V2 and V3**. *J Neurosci* 2016, **36**:1841-1857.

17. Krüger G, Kastrup A, Glover GH: **Neuroimaging at 1.5T and 3.0T: comparison of oxygenation-sensitive magnetic resonance imaging**. *Magn Reson Med* 2001, **45**:595-604.

18. • Triantafyllou C, Hoge RD, Krueger G, Wiggins CJ, Potthast A, Wiggins GC, Wald LL: **Comparison of physiological noise at 1.5T, 3T and 7T and optimization of fMRI acquisition parameters**. *Neuroimage* 2005, **26**:243-250.

This study addressed the question of whether the increasing physiological noise in BOLD fMRI with increasing field strength would counteract the expected sensitivity gains. Because small fMRI voxels have reduced physiological noise contributions and instead are thermal-noise dominated, high-resolution fMRI acquisitions enjoy the expected boost in sensitivity with higher field strengths. This study recommended small voxel sizes for UHF-fMRI, otherwise if larger voxels are used there may be little to no benefit of moving from 3T to 7T.

19. Triantafyllou C, Polimeni JR, Wald LL: **Physiological noise and signal-to-noise ratio in fMRI with multi-channel array coils**. *Neuroimage* 2011, **55**:597-606.

20. • Błażejewska AI, Fischl B, Wald LL, Polimeni JR: **Intracortical smoothing of small-voxel fMRI data can provide increased detection power without spatial resolution losses compared to conventional large-voxel fMRI data**. *Neuroimage* 2019, **189**:601-614.

Smaller fMRI voxel sizes reduce partial volume effects, allowing the voxels to sample more gray matter, leading to less noise contributions from surrounding CSF and less signal dilution from surrounding white matter. This study demonstrated that, perhaps surprisingly, small-voxel fMRI with advanced anatomically informed smoothing can provide higher overall sensitivity than conventional large-sized voxels.

21. Wiesinger F, Van de Moortele P-F, Adriany G, De Zanche N, Uğurbil K, Pruessmann KP: **Parallel imaging performance as a function of field strength—an experimental investigation using electrodynamic scaling**. *Magn Reson Med* 2004, **52**:953-964.

22. Keil B, Wald LL: **Massively parallel MRI detector arrays**. *J Magn Reson* 2013, **229**:75-89.

23. Uğurbil K, Auerbach E, Moeller S, Grant A, Wu X, Van de Moortele P-F, Olman C, DelaBarre L, Schillak S, Radder J *et al.*: **Brain imaging with improved acceleration and SNR at 7 Tesla obtained with 64-channel receive array**. *Magn Reson Med* 2019, **82**:495-509.

24. Polimeni JR, Bhat H, Witzel T, Benner T, Feiweier T, Inati SJ, Renvall V, Heberlein KA, Wald LL: **Reducing sensitivity losses due to respiration and motion in accelerated echo planar imaging by reordering the autocalibration data acquisition**. *Magn Reson Med* 2016, **75**:665-679.

25. Talagala SL, Sarlls JE, Liu S, Inati SJ: **Improvement of temporal signal-to-noise ratio of GRAPPA accelerated echo planar imaging using a FLASH based calibration scan**. *Magn Reson Med* 2016, **75**:2362-2371.

26. Lyu M, Liu Y, Wu EX: **Improved parallel imaging reconstruction of EPI using inversely distortion corrected FLASH as calibration data**. *Proc Intl Soc Mag Reson Med* 2018, **26**:3509.

27. Hoge WS, Polimeni JR: **Dual-polarity GRAPPA for simultaneous reconstruction and ghost correction of echo planar imaging data**. *Magn Reson Med* 2016, **76**:32-44.

28. Xie VB, Lyu M, Liu Y, Feng Y, Wu EX: **Robust EPI nyquist ghost removal by incorporating phase error correction with sensitivity encoding (PEC-SENSE)**. *Magn Reson Med* 2018, **79**:943-951 http://dx.doi.org/10.1002/mrm.26710.

29. Błażejewska AI, Bhat H, Wald LL, Polimeni JR: **Reduction of across-run variability of temporal SNR in accelerated EPI time-series data through FLEET-based robust autocalibration**. *Neuroimage* 2017, **152**:348-359.

30. Liu J, de Zwart JA, van Gelderen P, Murphy-Boesch J, Duyn JH: **Effect of head motion on MRI B0 field distribution**. *Magn Reson Med* 2018, **80**:2538-2548.

31. Dymerska B, Poser BA, Bogner W, Visser E, Eckstein K, Cardoso P, Barth M, Trattnig S, Robinson SD: **Correcting dynamic distortions in 7T echo planar imaging using a jittered echo time sequence**. *Magn Reson Med* 2016, **76**:1388-1399.

32. Dymerska B, Poser BA, Barth M, Trattnig S, Robinson SD: **A method for the dynamic correction of B0-related distortions in single-echo EPI at 7T**. *Neuroimage* 2018, **168**:321-331.

33. Wallace TE, Polimeni JR, Stockmann JP, Hoge WS, Kober T, Warfield SK, Afacan O: **Dynamic distortion correction for functional MRI using FID navigators**. *Magn Reson Med* 2021, **85**:1294-1307 http://dx.doi.org/10.1002/mrm.28505.

34. Andersson JLR, Graham MS, Drobnjak I, Zhang H, Campbell J: **Susceptibility-induced distortion that varies due to motion: correction in diffusion MR without acquiring additional data**. *Neuroimage* 2018, **171**:277-295.

35. Wilm BJ, Barmet C, Pavan M, Pruessmann KP: **Higher order reconstruction for MRI in the presence of spatiotemporal field**

perturbations. *Magn Reson Med* 2011, **65**:1690-1701 http://dx.doi.org/10.1002/mrm.22767.

36. Bollmann S, Kasper L, Vannesjo SJ, Diaconescu AO, Dietrich BE, Gross S, Stephan KE, Pruessmann KP: **Analysis and correction of field fluctuations in fMRI data using field monitoring**. *Neuroimage* 2017, **154**:92-105.

37. Juchem C, Umesh Rudrapatna S, Nixon TW, de Graaf RA: **Dynamic multi-coil technique (DYNAMITE) shimming for echo-planar imaging of the human brain at 7 Tesla**. *Neuroimage* 2015, **105**:462-472.

38. Stockmann JP, Wald LL: **In vivo B0 field shimming methods for MRI at 7T**. *Neuroimage* 2018, **168**:71-87.

39. Todd N, Josephs O, Callaghan MF, Lutti A, Weiskopf N: **Prospective motion correction of 3D echo-planar imaging data for functional MRI using optical tracking**. *Neuroimage* 2015, **113**:1-12.

40. Zaitsev M, Akin B, LeVan P, Knowles BR: **Prospective motion correction in functional MRI**. *Neuroimage* 2017, **154**:33-42.

41. Krause F, Benjamins C, Eck J, Lührs M, Hoof R, Goebel R: **Active head motion reduction in magnetic resonance imaging using tactile feedback**. *Hum Brain Mapp* 2019, **40**:4026-4037.

42. Power JD, Silver BM, Silverman MR, Ajodan EL, Bos DJ, Jones RM: **Customized head molds reduce motion during resting state fMRI scans**. *Neuroimage* 2019, **189**:141-149.

43. Polimeni JR, Wald LL: **Magnetic resonance imaging technology — bridging the gap between noninvasive human imaging and optical microscopy**. *Curr Opin Neurobiol* 2018, **50**:250-260.

44. Winkler SA, Schmitt F, Landes H, DeBever J, Wade T, Alejski A, Rutt BK: **Gradient and shim technologies for ultra high field MRI**. *Neuroimage* 2018, **168**:59-70.

45. Roemer PB, Edelstein WA, Hayes CE, Souza SP, Mueller OM: **The NMR phased array**. *Magn Reson Med* 1990, **16**:192-225.

46. Wald LL, Polimeni JR: **Impacting the effect of fMRI noise through hardware and acquisition choices – implications for controlling false positive rates**. *Neuroimage* 2017, **154**:15-22.

47. Faraji-Dana Z, Tam F, Chen JJ, Graham SJ: **Interactions between head motion and coil sensitivity in accelerated fMRI**. *J Neurosci Methods* 2016, **270**:46-60.

48. Patriat R, Reynolds RC, Birn RM: **An improved model of motion-related signal changes in fMRI**. *Neuroimage* 2017, **144**:74-82.

49. Gonzalez-Castillo J, Roopchansingh V, Bandettini PA, Bodurka J: **Physiological noise effects on the flip angle selection in BOLD fMRI**. *Neuroimage* 2011, **54**:2764-2778.

50. • Glasser MF, Sotiropoulos SN, Wilson JA, Coalson TS, Fischl B, Andersson JL, Xu J, Jbabdi S, Webster M, Polimeni JR *et al.*: **The minimal preprocessing pipelines for the Human Connectome Project**. *Neuroimage* 2013, **80**.
This article describes best-practice functional MRI data preprocessing and analysis procedures that were developed for the Human Connectome Project. The rationale behind these recommendations is to maintain geometric accuracy of the data, and several approaches that can circumvent inadvertent spatial resolution loss are summarized.

51. Pur DR, Eagleson RA, de Ribaupierre A, Mella N, de Ribaupierre S: **Moderating effect of cortical thickness on BOLD signal variability age-related changes**. *Front Aging Neurosci* 2019, **11**:46.

52. • Viessmann O, Scheffler K, Bianciardi M, Wald LL, Polimeni JR: **Dependence of resting-state fMRI fluctuation amplitudes on cerebral cortical orientation relative to the direction of B0 and anatomical axes**. *Neuroimage* 2019, **196**:337-350.
This study demonstrated that, because of the coupling between vascular geometry and cerebral cortical geometry, the largest cortical vessels run along the cortical surface, which imparts a 'cortical orientation effect' on the BOLD fMRI signal. The cortical orientation effect causes resting-state BOLD fluctuation amplitudes to be systematically larger in regions where the cortical surface normal is parallel to the main magnetic field direction, and this effect can be up to 70% at 7T.

53. Gagnon L, Sakadžić S, Lesage F, Musacchia JJ, Lefebvre X, Fang Q, Yücel MA, Evans KC, Mandeville ET, Cohen-Adad J *et al.*: **Quantifying the microvascular origin of bold-fMRI from first principles with two-photon microscopy and an oxygen-sensitive nanoprobe**. *J Neurosci* 2015, **35**:3663-3675.

54. Bernier M, Cunnane SC, Whittingstall K: **The morphology of the human cerebrovascular system**. *Hum Brain Mapp* 2018, **39**:4962-4975.

55. de Bertoldi F, Finos L, Maieron M, Weis L, Campanella M, Ius T, Fadiga L: **Improving the reliability of single-subject fMRI by weighting intra-run variability**. *Neuroimage* 2015, **114**:287-293.

56. •• Szinte M, Knapen T: **Visual organization of the default network**. *Cereb Cortex* 2020, **30**:3518-3527.
This recent study demonstrated that 30 runs of BOLD-fMRI data from two individual subjects at 7T produced comparable results to a 181-subject average. These results indicated that, in this example at least, an order of magnitude less time and resources are required to achieve sufficient sensitivity in a single-subject study compared to a group-level study.

57. D'Esposito M: **Are individual differences in human brain organization measured with functional MRI meaningful?** *Proc Natl Acad Sci U S A* 2019, **116**:22432-22434.

58. Berman AJL, Grissom WA, Witzel T, Nasr S, Park DJ, Setsompop K, Polimeni JR: **Ultra-high spatial resolution BOLD fMRI in humans using combined segmented-accelerated VFA-FLEET with a recursive RF pulse design**. *Magn Reson Med* 2021, **85**:120-139.

59. Heidemann RM, Ivanov D, Trampel R, Fasano F, Meyer H, Pfeuffer J, Turner R: **Isotropic submillimeter fMRI in the human brain at 7T: combining reduced field-of-view imaging and partially parallel acquisitions**. *Magn Reson Med* 2012, **68**:1506-1516.

60. Lewis LD, Setsompop K, Rosen BR, Polimeni JR: **Fast fMRI can detect oscillatory neural activity in humans**. *Proc Natl Acad Sci U S A* 2016, **113**:E6679-E6685.

61. Uludağ K, Müller-Bierl B, Uğurbil K: **An integrative model for neuronal activity-induced signal changes for gradient and spin echo functional imaging**. *Neuroimage* 2009, **48**:150-165.

62. Huber L, Uludağ K, Möller HE: **Non-BOLD contrast for laminar fMRI in humans: CBF, CBV, and CMRO2**. *Neuroimage* 2019, **197**:742-760.

63. •• Botvinik-Nezer R, Holzmeister F, Camerer CF, Dreber A, Huber J, Johannesson M, Kirchler M, Iwanir R, Mumford JA, Adcock RA *et al.*: **Variability in the analysis of a single neuroimaging dataset by many teams**. *Nature* 2020, **582**:84-88.
This recent study underscores the importance of fMRI data preprocessing and the profound influence it can have on the final results, especially in the context of high-resolution fMRI. Here the authors provided an fMRI dataset to 70 independent research teams, and the high variability of the results across the teams was attributed mainly to differences in preprocessing strategies, specifically to differences in spatial smoothness and that 'the relevant smoothness arose from analytical steps beyond explicit smoothing'.

64. Polimeni JR, Renvall V, Zaretskaya N, Fischl B: **Analysis strategies for high-resolution UHF-fMRI data**. *Neuroimage* 2018, **168**:296-320.